applied sciences

MDPI

Article

Photo-Aligned Nematic Liquid Crystals Enable the Modulation of Thermoplasmonic Heating

Giovanna Palermo [1,2,*], Rossella Grillo [3,4], Luigia Pezzi [1,2], Thomas Bürgi [3], Nelson Tabiryan [5], Luciano De Sio [2,6] and Cesare Umeton [1,*]

1 Department of Physics, University of Calabria, Via P. Bucci, 87036 Rende, Italy; luigia.pezzi@fis.unical.it
2 CNR NANOTEC—Istituto di Nanotecnologia, UOS Cosenza, 87036 Rende, Italy; luciano.desio@uniroma1.it
3 Department of Physical Chemistry, University of Geneva, 41211 Geneva, Switzerland; rossella.grillo@unirc.it (R.G.); Thomas.Buergi@unige.ch (T.B.)
4 DIIES Department, Mediterranea University of Reggio Calabria, Loc. Feo di Vito, 89122 Reggio Calabria, Italy
5 Beam Engineering for Advanced Measurements Company, 1300 Lee Road, Orlando, FL 32789, USA; nelson@beamco.com
6 Department of Medico-Surgical Sciences and Biotechnologies, Center for Biophotonics, Sapienza University of Rome, Corso Della Repubblica 79, 04100 Latina, Italy
* Correspondence: giovanna.palermo@unical.it (G.P.); cesare.umeton@fis.unical.it (C.U.)

Abstract: We experimentally demonstrate that the plasmonic heat delivered by a single layer of homogeneously distributed gold nanoparticles (AuNPs), immobilized on a glass substrate, can be optically tuned by taking advantage of the properties of an organic layer based on azobenzene and nematic liquid crystal (NLC) molecules. The effect, which exploits the dependence of the NLC refractive index value on the molecular director orientation, is realized using the polarization-dependent, light-induced molecular reorientation of a thin film of photo-aligning material that the NLC is in contact with. The reversibility of the optically induced molecular director reorientation of the NLC enables an active modulation of the plasmonic photo-induced heat.

Keywords: thermoplasmonics; metallic nanoparticles; liquid crystals; reconfigurability; photo-aligning materials

check for updates

Citation: Palermo, G.; Grillo, R.; Pezzi, L.; Bürgi, T.; Tabiryan, N.; De Sio, L.; Umeton, C. Photo-Aligned Nematic Liquid Crystals Enable the Modulation of Thermoplasmonic Heating. *Appl. Sci.* **2021**, *11*, 6272. https://doi.org/10.3390/app11146272

Academic Editor: Gaetano Assanto

Received: 29 May 2021
Accepted: 5 July 2021
Published: 7 July 2021

Publisher's Note: MDPI stays neutral with regard to jurisdictional claims in published maps and institutional affiliations.

Copyright: © 2021 by the authors. Licensee MDPI, Basel, Switzerland. This article is an open access article distributed under the terms and conditions of the Creative Commons Attribution (CC BY) license (https://creativecommons.org/licenses/by/4.0/).

1. Introduction

Thermoplasmonics has become one of the most renowned research topics in plasmonics and nano-optics, thanks to the possibility of generating and controlling a great amount of heat at the nanoscale. Thermoplasmonics deals with the heat produced by metallic nanoparticles (NPs) when a radiation with suitable (resonant) wavelength impinges on them [1,2]. Indeed, when the electrons of the conduction band of a metallic NP oscillate coherently with the electric field of the incident radiation, an increase of the absorption in the corresponding frequency range occurs (ω_p) that leads to a rapid rise in the temperature of the NP, followed by a heat dissipation into surrounding media [3,4]. The temperature increase (ΔT) of a single spherical NP can be easily expressed as $\Delta T = Q/(4\pi k_H R_{NP})$, where R_{NP} is the NP radius, k_H is the thermal conductivity of the host medium, and Q is the heat power density. Q depends on the absorption cross-section (σ_{abs}) of the NP, and on the intensity (I) of the incident light through the equation: $Q = \sigma_{abs}\ I$ [1–4]. For a metallic NP with spherical or rod-like shape, σ_{abs} can be easily calculated using the Mie or Gans theories, respectively, ref. [1–4] while for different geometries more complex theoretical models are required. Nowadays, the thermoplasmonic heating is used in several research fields such as high precision medicine [5–7], electronics [8–10] optics [11–13], biology [14,15], and catalysis [16,17]. All above applications are based on the possibility to finely tune the photo-thermal efficiency of the NPs that can be done by acting on several control parameters such as the intensity of the impinging beam [1–4], the number (N) of involved NPs, and the dielectric function of the surrounding medium ε_H [18]. The latter

can be achieved by exploiting the properties of smart and thermo-responsive materials such as thermotropic liquid crystals (LCs). These are organic and anisotropic materials responsive to different external perturbations such as electric, optical and magnetic fields, and temperature variation. LCs have been largely used in various research fields ranging from displays [19–21] to plasmonics [22,23]. Notably, the temperature sensitivity of the optical properties of LCs have been used as a compelling solution to realize novel methodologies for monitoring and controlling the light-induced heat of NPs [24]. In this work, we report and discuss on the realization of a thermoplasmonic-based optical device made of an array of gold nanoparticles (AuNPs) immobilized on a glass substrate and layered with a photo-aligned NLC. This hybrid system, which represents an all-optical thermoplasmonic device, ingeniously realized through the combination of hard-matter (plasmonic NPs) and soft matter (LCs), is characterized in terms of morphological, optical, and thermo-optical properties. It turns out that the thermoplasmonic heating can be easily controlled by controlling the refractive index of the surrounding LC medium, thanks to the presence of the thin surface command layer. Indeed, starting from a single layer of metal NPs the photothermal response can be controlled by varying the intensity in a specific range, but also with the same power of the resonant radiation through subtle control of the refractive index of the surrounding medium, obtainable using the photo-aligning material and liquid crystal. The all-optical thermoplasmonic device forecasts exciting applications in the field of light-driven thermoplasmonics.

2. Materials and Methods

Synthesis of spherical gold nanoparticles: Spherical gold nanoparticles have been prepared according to the conventional Turkevich method [25]. This is the most commonly used approach for the synthesis of size-defined spherical gold nanoparticles through chemical reduction by sodium citrate. Briefly, in a round-bottomed flask, 600 mL of an aqueous solution of tetrachloroauric (III) acid (0.25 mM) were brought to boiling under vigorous magnetic stirring. When the boiling temperature was reached, the gold has been reduced by quickly adding 15 mL of aqueous sodium citrate solution (0.03 M). In about 15 min, the solution colour slowly turned from yellow to deep red, as a result of the full reduction of the gold salt into monodisperse gold nanoparticles with an average diameter of 20 nm. The reaction was then removed from the hot oil bath and allowed to cool down to room temperature overnight.

Functionalization of substrates: The glass substrates were cleaned and hydroxylated with piranha solution (3:1 mixture of sulphuric acid to hydrogen peroxide 30%) for 30 min. Then, the substrates were rinsed several times, first with distilled water and then with milli-Q water before being dried under nitrogen flow. To alter the surface chemistry, the substrates were immersed in a 5% (v/v) solution of N-[3-(trimethoxysilyl)propyl] ethylenediamine in ethanol for 30 min and then rinsed with milli-Q water. Excess of water was removed using a stream of nitrogen followed by drying in a furnace at 120 °C for 30 min to assure good silanization.

Gold nanoparticles arrays on planar substrates: Gold nanoparticles were deposited on glass slides by immersing the functionalized substrates in the colloidal solution for two and a half hours. The gold covered substrates were then washed with milli-Q water and dried under a stream of nitrogen.

Deposition of the photoaligning material: PAAD-27 by BeamCo. dissolved in dimethylformamide (C_3H_7NO), which possesses a broad absorption band centered at 415 nm, has been deposited by means of a spin coater (2000 rpm for 30 s). A polarized UV lamp (λ = 395 nm; I = 30 mW/cm^2) is used for a suitable time interval (typically 7 min) to reorient the PAAD-27 molecules perpendicularly to its polarization direction. The characteristics average polar anchoring energies of nematic LC on PAAD materials (Beamco., Orlando, FL, USA) are $\approx 10^{-2}$ J/m^2, a weaker alignment than on polyimide layer [26].

Preparation of the sample cell: The thermotropic nematic liquid crystal (NLC) E7, by Merck has been used. The sample cell was fabricated by gluing together a functionalized

glass slide and the PAAD-27 coated AuNPs monolayer, spaced by 10 µm glass microspheres. The NLC has been then introduced by means of capillary flow. The surface of the glass substrate is covered with a thin organic film, such as polyimide (PI-AL1454 by JSR), using a spin coating (4000 rpm, 60 s) deposition technique. After the deposition of the coating film, a cloth (velvet) with short fibers is moved over the surface to create microgrooves that make the surface unidirectionally anisotropic. The rubbing process induces a specific orientation of the polymer molecules, which is transmitted to the LC molecules anchored on the substrates; moreover, this kind of orientational order propagates in the bulk of the LC molecules via intermolecular forces [27].

Thermographic analysis: The thermographic analysis has been performed by means of a thermocamera (E40 by FLIR), which is characterized by a sensitivity of 0.07 °C and a spatial resolution of 2.72 mrad. The steady-state condition was reached after about 5 min of exposure of the sample cell to a green laser beam (λ = 532 nm) —Verdi G-Series by Coherent, linearly polarized—polarization direction: vertical, $\pm 5^{\circ}$, when no further temperature variations were detected in the limit of the thermo-camera sensitivity.

3. Results and Discussion

AuNPs monolayers on glass substrates have been prepared by following the procedure described in the Materials and Methods section. The samples were then characterized by performing a morphological analysis by means of an Atomic Force Microscope (AFM). Figure 1a shows a representative AFM image of uniformly distributed AuNPs with an average diameter of about 20 nm. The inset of Figure 1a shows a photo of the realized sample, which exhibits a distinctive pinkish color associated with the presence of well-dispersed AuNPs. Indeed, the spectral response of the sample (Figure 1b) shows the typical absorption peak of spherical AuNPs centered at the wavelength λ_{LPR} = 522 nm, corresponding to the localized plasmon resonance of the AuNPs [1,2]. Figure 1c shows the absorption spectrum of the photoaligning material PAAD-27 (by BeamCo), dissolved in dimethylformamide, which possesses a broad absorption band centered at 420 nm. PAAD-27 is an azo-based material that is used to promote planar alignment of nematic liquid crystals (NLC); its optical and all-optical properties have been reported elsewhere [28,29].

The AuNPs monolayer has been then covered with the PAAD-27 material (see Materials and Methods section): the absorbance of the obtained sample (AuNPs + PAAD 27) is reported in Figure 1d (green curve). The absorption peak of AuNPs is significantly red shifted, from 522 nm to 544 nm. In general, when metallic nanoparticles are immersed in a large refractive index medium, the resonance is shifted toward longer wavelengths [30]. In fact, the shift observed in Figure 1d is related to a change in the refractive index n of the surrounding medium: from the air value (n_{air} = 1) to the PAAD-27 value (n_{PAAD} = 1.73). This behavior well agrees with the Mie theory [31], which provides an analytical solution of Maxwell's equations used to calculate the scattering and the absorption of electromagnetic radiation due to a spherical and isolated metallic NP. Figure 2a sketches the AuNPs monolayer on glass substrate before (top-left) and after the deposition of the PAAD-27 (top-right), whose molecules are randomly aligned. When the sample is illuminated with a polarized UV light (10 min, 2.7 J/cm^2), a PAAD-27 molecular alignment is induced, which turns out to be perpendicular to the light polarization direction. In fact, when PAAD-27 molecules are optically activated by a light beam whose polarization direction is parallel to their absorption oscillators, they become excited and relax several times with a random alignment; this process results in a new orientation of the PAAD molecules with respect to the initial one, with a consequent excess of molecules in the direction in which the absorbing oscillators are perpendicular to the polarization of the incident radiation. It is a consequence of this process that the PAAD-27 alignment direction can be easily modified by changing the polarization direction of the incident UV light beam. Figure 2b highlights that once the sample is exposed to polarized UV radiation, a further red shift of the plasmonic band is observed with respect to the position registered for the sample in which the AuNPs are covered by amorphous (not aligned) PAAD-27; this further red shift of about 16 nm

can be attributed to the change of the refractive index of the medium surrounding the AuNPs, following the alignment of the PAAD-27 molecules. Finally, we have observed that there is no difference in the shift of the plasmonic band of the sample covered with a PAAD-27 layer when this is acted on by radiations with different (orthogonal) polarizations (blue and magenta curves of Figure 2b). This result points out that the plasmonic response of the AuNPs is not substantially affected by the actual in-plane orientation of the PAAD-27 molecules.

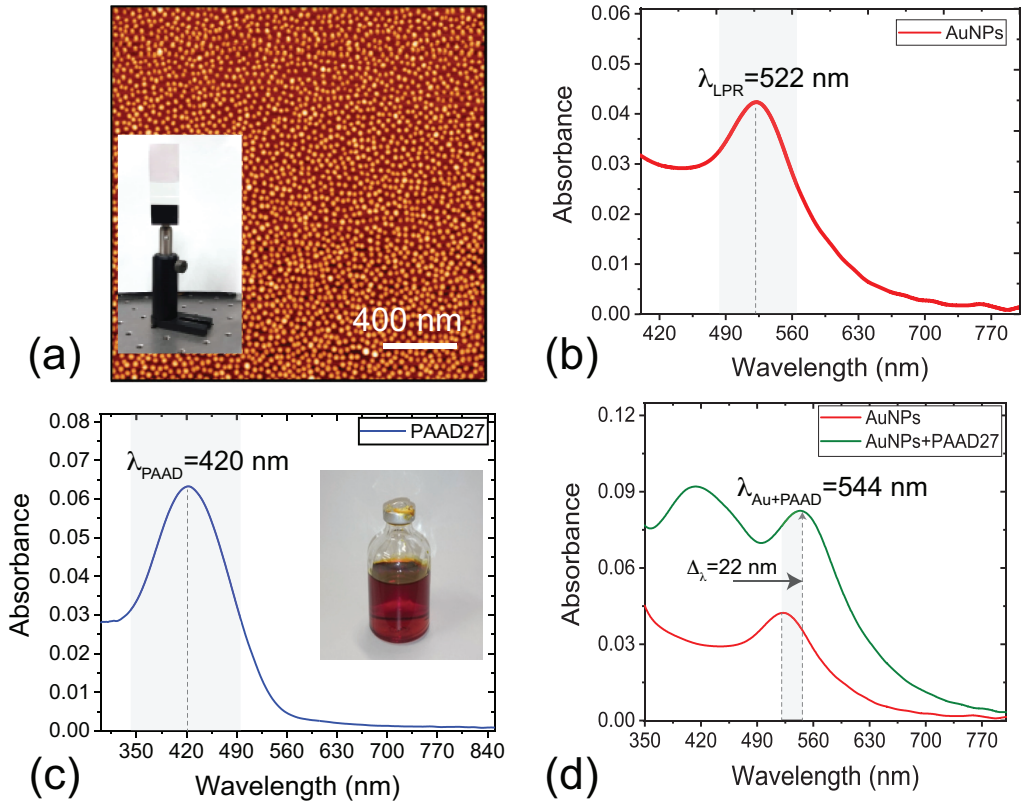

Figure 1. (**a**) AFM image of the AuNPs monolayer on a glass substrate. In the inset, a photograph of the sample. Spectral response of the AuNPs monolayer surrounded by (**b**) air and (**c**) PAAD-27; In the inset, a photograph of the photo-aligning material. (**d**) Absorbance response of the AuNPs monolayer covered by the PAAD-27.

A very interesting behavior is observed when monitoring the photothermal response of the sample. The thermo-optical setup used for the experiments is sketched in Figure 2c: A CW green laser (λ = 532 nm, spot size 2.25 $\pm$ 0.22 mm), impinges perpendicularly onto the sample and excites simultaneously the plasmonic band of the irradiated AuNPs, with a consequent increase (ΔT) of the macroscopic temperature of the sample with respect to the environment temperature (T_0). In general, to calculate the temperature variation at a point r from a single NP, it is necessary to solve the heat transfer equation [4], where the solution results are:

$$\Delta T(r) = \frac{QR_{NP}^3}{3rk_H} \quad (1)$$

where Q is the heat production due to the Joule effect, R_{NP} is the NP radius and K_H is the thermal conductivity of the host medium. Thus, by illuminating a macroscopic surface region of the AuNPs layer with a laser spot w in radius, a considerable number of AuNPs are acted on by the light; in this case, as a matter of fact, the temperature increase has to be calculated by adding the contribution of all the irradiated AuNPs as specified in this formula [18]:

$$\Delta T(r) = 2\pi w n_{NP} \frac{V_{NP} Im(\chi_{NP})}{2\lambda k_H \sqrt{\varepsilon_H}} \left| \frac{3\varepsilon_H}{2\varepsilon_H + \varepsilon_{NP}} \right|^2 I \quad (2)$$

where n_{NP} is the AuNPs surface density, V_{NP} is the average AuNP volume, K_H is the thermal conductivity of the host medium, χ_{NP} is the AuNPs dielectric permeability, ε_{NP} and ε_H are the AuNPs and host medium dielectric permittivity, respectively. From Equation (2), it is evident that the temperature variation exhibits a strong enhancement under the Frölich condition, in which the quantity $|2\varepsilon_H + \varepsilon_{NP}|$ assumes a minimum value, a condition that occurs if $Re[\varepsilon_{NP}(\omega)] = -2\varepsilon_H$ [32]. Equation (2) shows also that the temperature variation ΔT varies linearly with the intensity of the pump beam (I), used to excite the resonance of the AuNPs, and strongly depends on the optical and thermal characteristics of the medium that hosts the AuNPs, expressed by ε_H and k_H, respectively. This behavior was experimentally demonstrated by illuminating the AuNPs with different pump beam intensities I and by monitoring the maximum induced ΔT for each I value. By monitoring the temperature values T_{max} of the central pixel of each hot-spot of the thermographic images (Figure 2c), which corresponds to the warmest point, we plotted the temperature variation $\Delta T = T_{max} - T_0$ versus the impinging intensity I. Successively, we repeated the photothermal experiments (Figure 2d) by fixing the intensity range ($I = 0.05 - 1.2$ W/cm^2) for the cases of AuNPs monolayer in air (red sphere) and covered by the PAAD-27 molecules before (green sphere) and after exposure to UV light of two different polarization directions (blue and magenta spheres). As predicted by Equation (2), the behavior of ΔT as a function of I can be easily fitted with a linear curve. For the maximum I considered we acquire a ΔT of about (3.2 ± 0.3) °C for the AuNPs monolayer in air, (32.6 ± 0.3) °C for the sample where AuNPs are covered by PAAD-27, and of about (49.0 ± 0.3) °C and (38.0 ± 0.3) °C for AuNPs-PAAD-27 samples acted on by UV light with two different polarization directions. The differences in the measured ΔT values acquired for the four different cases is related to the variation of the AuNPs plasmonic band induced by changes in the characteristics of the host medium surrounding the AuNPs. In particular, Figure 2b shows that in the case of not aligned PAAD-27, there is an increase of the sample absorbance, and this is also observed when the PAAD-27 molecules are aligned. However, in this latter case, the difference in the temperature variations are not due to a change in the sample absorbance but to a different value of k_H in the two cases: as a matter of fact, the observation that the plasmonic band does not change for the two different alignment conditions indicates that no variations occur in the refractive index of the PAAD-27, which corresponds to no variation in the Frölich condition. Therefore, a prediction of the sample temperature variation goes through a determination of the k_H value of the medium hosting the AuNPs, which is made of glass and PAAD-27 layer. We can say that the PAAD-27 alignment induces a reversible and repeatable thermal anisotropy due to an induced change in the thermal conductivity value of the PAAD-27, which turns out to be different for the two different polarization directions of the resonant impinging light. As demonstrated in a previous work [18], we are able to calculate the thermal conductivity value by detecting variations of sample temperature as a function of the laser intensity; thus, we can determine the thermal anisotropy of the PAAD-27 layer using Equations (1) and (2). Following the procedure illustrated in [18], the k_H values of the PAAD-27 in the three cases are measured as: 0.77 W(° m)$^{-1}$ for the amorphous PAAD-27, 0.32 W(° m)$^{-1}$ for the E_x aligned PAAD-27 and 0.40 W(° m)$^{-1}$ for the E_y aligned PAAD-27. These results confirm that it is possible to modulate the thermal behavior of PAAD-27 material by means of polarized light. As mentioned above, PAAD-27 can be used to align liquid crystals; for this reason, we have studied the behavior of a sample of AuNPs + PAAD-27 modified by adding a nematic liquid crystal (NLC, see Materials and Methods section) to investigate how a variation of the optical properties of the new medium (represented now by PAAD-27 plus NLC) surrounding the AuNPs, determines variations of the thermal efficiency of the whole system that are not related to a change in the value of the thermal conductivity k_H of some of its components.

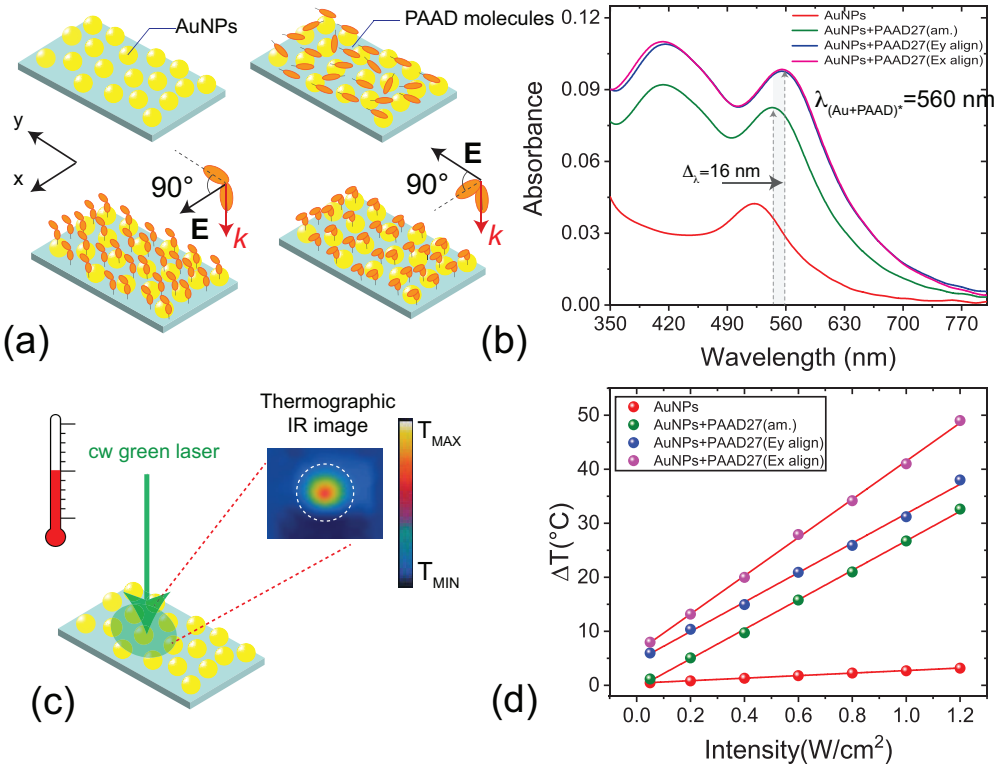

Figure 2. (**a**) Sketch of the AuNPs monolayer on a glass substrate before (top, left) and after the deposition of the PAAD-27 material (top, right); orientation of the PAAD-27 molecules after the exposure to UV radiation for two different polarizations (bottom). (**b**) Absorbance response of the AuNPs monolayer in the air (red curve), after the deposition of the PAAD-27—before (green curve) and after the exposure to polarized UV radiation with different polarizations (blue and magenta curves); (**c**) Sketch of the photothermal measurement. (**d**) Photo-thermal response of the AuNPs monolayer in air and after the deposition and alignment of the PAAD-27.

A sketch of the photo-alignment process of the NLC molecules is reported in Figure 3a. Two limit cases are considered for the configuration of the NLC director as determined by the PAAD-27 photalignement: a planar one, in which the directions of the molecular director on the two sides of the cell are parallel to each other, and a twisted one, in which these directions are perpendicular to each other; details on cell fabrication are reported in the Materials and Methods section. Figure 3b shows polarized optical microscope (POM) images of the photo-exposed area of the sample. The original planar aligned area is outside the red circled zone, while inside, there is a twisted aligned area after it has been exposed to an external light source for 7 min (λ_{max} = 405 nm; I = 30 mW/cm^2). The spectral response of the sample shows a decrease of the absorbance in the plasmonic band and a blue shift with respect to the AuNPs+PAAD-27 sample (Figure 3c). This behavior can be ascribed to a reduction of the effective refractive index that the AuNPs monolayer sees in the surrounding medium in both (planar and twisted) alignment configurations due to the presence of the NLC. As a consequence, the corresponding temperature variation results are lower with respect to the sample with PAAD-27 alone (Figure 3d) but still totally tunable in a given range. In fact, the ΔT obtained at the maximum intensity of the impinging light are about (13.0 $\pm$ 0.3) °C for the planar cell and (28.2 $\pm$ 0.3) °C for the twisted cell. Interestingly, all intermediate temperature variations highlighted in Figure 3d by the yellow region can be obtained by continuously varying the polarization of the aligning UV light which reorients the PAAD-27 and therefore the NLC director from the planar to twisted cases.

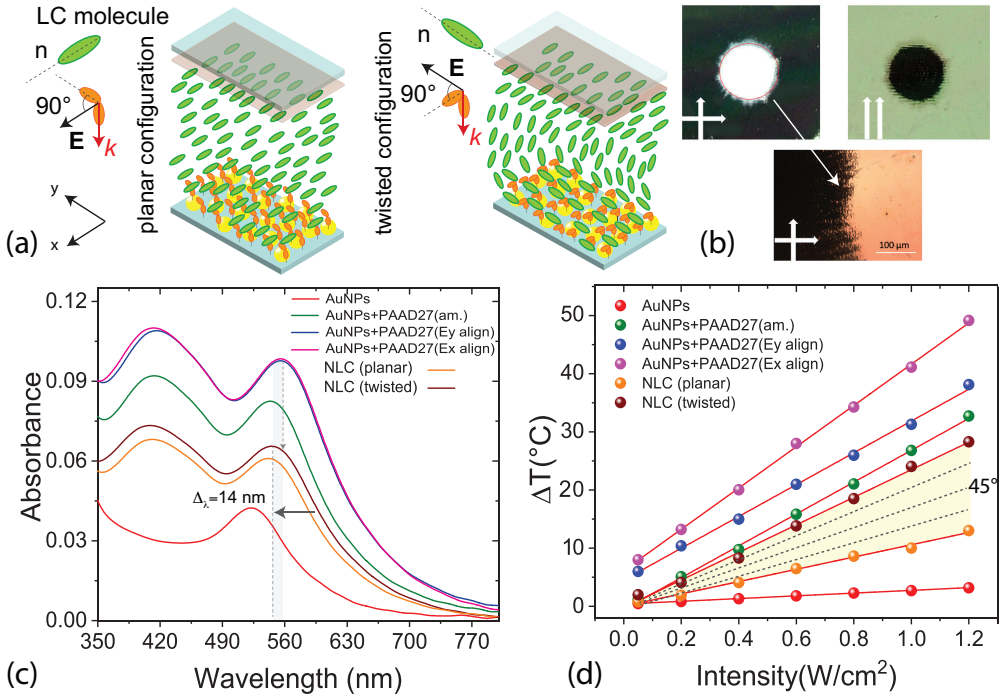

Figure 3. (**a**) Sketch of the AuNPs+PAAD-27+NLC cell in planar and twisted configuration. (**b**) POM view of the planar (left and right images, outside the red circle) and twist (left and right images, inside the red circle) alignment along with a high magnification of the transition zone (from planar to twist, bottom photo) of the sample. Left and right images have been acquired between crossed and parallel polarizers, respectively. (**c**) Absorbance of the AuNPs monolayer in air, covered by PAAD-27 and with NLC; (**d**) Photo-thermal response of the sample in air and after the deposition and alignment of PAAD-27 and the infiltration and photo-alignment of NLC.

As we can see in Table 1, the combination of an AuNPs layer with a photoaligning material as PAAD-27, demonstrates the potential response of the system to the change of the refractive index of the surrounding medium. From the linear fit of the temperature variation ΔT as a function of the intensity of the pump beam, it is possible to calculate the Sensitivity (α) of the system, defined as $\Delta T/\Delta I$, representing the slope of the linear fit. This parameter can help to better understand the performance of the proposed device; just an example: the highest thermal response is obtained in the case of AuNPs + PAAD-27 Ex aligned characterized by a sensitivity of (35.38 ± 0.41) °C m^2/W; if, on the other hand, it is necessary to have greater control of the temperature in a very precise range and for a specific intensity range of the pump beam, the choice of inserting the liquid crystal in the system produces a higher thermal variation range if compared to the case of the PAAD-27 alone.

Table 1. Maximum temperature variation ΔT of the samples and the corresponding Sensitivity.

Sample	$\Delta T = T_{max} - T_0$ [°C]	α: Sensitivity ($\Delta T/\Delta I$) [°C m^2/W]
AuNPs	3.2 ± 0.3	2.35 ± 0.02
AuNPs + PAAD-27 amorphous	32.6 ± 0.3	9.43 ± 0.07
AuNPs + PAAD-27 Ex align.	49.0 ± 0.3	35.38 ± 0.41
AuNPs + PAAD-27 Ey. Align.	38.0 ± 0.3	27.26 ± 0.53
AuNPs + PAAD-27 + NLC (planar)	13.0 ± 0.3	10.95 ± 0.33
AuNPs + PAAD-27 + NLC (twisted)	28.2 ± 0.3	20.63 ± 0.43

4. Conclusions

We proved that: (a) by exploiting a photo-aligning material (PAAD-27) alone it is possible to modify the photo-thermal efficiency of a monolayer of gold nanoparticles (AuNPs); (b) the photo-aligning material, as driven by a polarized UV light, can be exploited to reorient the director of NLC molecules used as host medium of an AuNPs monolayer; this director reorientation induces a modification of the effective refractive index of the NLC as seen by the AuNPs; in turn, this variation affects the photothermal response of the monolayer of AuNPs. In particular, for the maximum intensity considered (I = 1.2 W/cm^2) a ΔT of about (3.2 $\pm$ 0.3) °C is detected for the AuNPs monolayer in air, (32.6 $\pm$ 0.3) °C for the sample where AuNPs are covered by PAAD-27, and of about (49.0 $\pm$ 0.3) °C and (38.0 $\pm$ 0.3) °C for AuNPs-PAAD-27 samples acted on by UV light of two different polarization directions. The presence of the PAAD-27 leads to a modulation of the photo thermal response whose photo-thermal range extension can be maximized using the PAAD-27 as photoaligning layer for NLC. In this case the ΔT obtained at the maximum intensity of the impinging light are about (13.0 $\pm$ 0.3) °C for the planar cell and (28.2 $\pm$ 0.3) °C for the twisted cell. In conclusion, we have shown that a particular interaction of light with nematic liquid crystals, mediated by a photo-aligning material, can be exploited to control an effect of thermoplasmonic heating. Indeed, by simply varying the polarization direction of the UV light that drives the reorientation of the NLC director (by means of photosensitive PAAD-27 molecules), it is possible to control in a simple and fast way the heat produced at the nanoscale by a monolayer of gold nanoparticles.

Author Contributions: G.P., L.D.S. and C.U. conceived the idea. G.P. fabricated and fully characterized the samples. R.G. and T.B. fabricated and characterized the metallic nanostructures. L.P. conceived and carried out the theoretical work. N.T. fabricated and characterized the photo aligning material. T.B., N.T. and C.U. supervised the work. G.P. and L.D.S. and C.U. prepared and wrote the manuscript with input from all authors. All authors reviewed the manuscript. All authors have read and agreed to the published version of the manuscript.

Funding: Not applicable.

Institutional Review Board Statement: Not applicable.

Informed Consent Statement: Not applicable.

Data Availability Statement: The data that support the findings of this study are available within the article.

Acknowledgments: This research has been supported by the "AIM: Attraction and International Mobility", PON R&I 2014-2020 Calabria.

Conflicts of Interest: The authors declare no conflict of interest.

References

1. Baffou, G.; Quidant, R. Thermo-plasmonics: Using metallic nanostructures as nano-sources of heat. *Laser Photonics Rev.* **2013**, *7*, 171–187. [CrossRef]
2. Baffou, G.; Quidant, R. Thermoplasmonics. In *World Scientific Handbook of Metamaterials and Plasmonics: Volume 4: Recent Progress in the Field of Nanoplasmonics*; World Scientific: Singapore, 2018; pp. 379–407.
3. Baffou, G.; Cichos, F.; Quidant, R. Applications and challenges of thermoplasmonics. *Nat. Mater.* **2020**, *19*, 946–958. [CrossRef] [PubMed]
4. Govorov, A.O.; Richardson, H.H. Generating heat with metal nanoparticles. *Nano Today* **2007**, *2*, 30–38. [CrossRef]
5. Lal, S.; Clare, S.E.; Halas, N.J. Nanoshell-enabled photothermal cancer therapy: Impending clinical impact. *Acc. Chem. Res.* **2008**, *41*, 1842–1851. [CrossRef] [PubMed]
6. Huang, X.; Jain, P.K.; El-Sayed, I.H.; El-Sayed, M.A. Plasmonic photothermal therapy (PPTT) using gold nanoparticles. *Lasers Med. Sci.* **2008**, *23*, 217–228. [CrossRef]
7. Guglielmelli, A.; Rosa, P.; Contardi, M.; Prato, M.; Mangino, G.; Miglietta, S.; Petrozza, V.; Pani, R.; Calogero, A.; Athanassiou, A.; et al. Biomimetic keratin gold nanoparticle-mediated in vitro photothermal therapy on glioblastoma multiforme. *Nanomedicine* **2020**, *16*, 121–138. [CrossRef]
8. Tordera, D.; Zhao, D.; Volkov, A.V.; Crispin, X.; Jonsson, M.P. Thermoplasmonic semitransparent nanohole electrodes. *Nano Lett.* **2017**, *17*, 3145–3151. [CrossRef]

9. Agarwal, D. Engineering Phonon, Photon, Electron and Plasmon Interactions in Silicon-Metal Nanocavitiies for Silicon Photonics and Thermoplasmonics. Ph.D. Thesis, University of Pennsylvania, Philadelphia, PA, USA, 2016.
10. Wang, S.; Komvopoulos, K. Effect of material optical properties on thermo-plasmonics of heat-assisted magnetic recording devices. *J. Appl. Phys.* **2018**, *124*, 185109. [CrossRef]
11. Pierini, F.; Guglielmelli, A.; Urbanek, O.; Nakielski, P.; Pezzi, L.; Buda, R.; Lanzi, M.; Kowalewski, T.A.; De Sio, L. Thermoplasmonic-Activated Hydrogel Based Dynamic Light Attenuator. *Adv. Opt. Mater.* **2020**, *8*, 2000324. [CrossRef]
12. Lio, G.E.; Ferraro, A.; Ritacco, T.; Aceti, D.M.; De Luca, A.; Giocondo, M.; Caputo, R. Leveraging on ENZ Metamaterials to Achieve 2D and 3D Hyper-Resolution in Two-Photon Direct Laser Writing. *Adv. Mater.* **2021**, *33*, 2008644. [CrossRef]
13. Cunha, J.; Guo, T.L.; Koya, A.N.; Toma, A.; Prato, M.; Della Valle, G.; Alabastri, A.; Proietti Zaccaria, R. Photoinduced Temperature Gradients in Sub-Wavelength Plasmonic Structures: The Thermoplasmonics of Nanocones. *Adv. Opt. Mater.* **2020**, *8*, 2000568. [CrossRef]
14. Zhu, M.; Baffou, G.; Meyerbrker, N.; Polleux, J. Micropatterning thermoplasmonic gold nanoarrays to manipulate cell adhesion. *ACS Nano* **2012**, *6*, 7227–7233. [CrossRef]
15. Shen, W.; Black, N.; Kalies, S.; Mazur, E. Impulse generated by laser-irradiated nanostructures in water and its effects on cell poration. *Plasmon. Biol. Med. Int. Soc. Opt. Photonics* **2021**, *11661*, 116610C.
16. Naldoni, A.; Kudyshev, Z.A.; Mascaretti, L.; Sarmah, S.P.; Rej, S.; Froning, J.P.; Tomanec, O.; Yoo, J.E.; Wang, D.; Kment, S.; et al. Solar thermoplasmonic nanofurnace for high-temperature heterogeneous catalysis. *Nano Lett.* **2020**, *20*, 3663–3672. [CrossRef]
17. Chehadi, Z.; Girardon, J.S.; Capron, M.; Dumeignil, F.; Jradi, S. Thermoplasmonic-induced energy-efficient catalytic oxidation of glycerol over gold supported catalysts using visible light at ambient temperature. *Appl. Catal. A Gen.* **2019**, *572*, 9–14. [CrossRef]
18. Pezzi, L.; Palermo, G.; Veltri, A.; Cataldi, U.; Bürgi, T.; Ritacco, T.; Giocondo, M.; Umeton, C.; De Luca, A. Photo-thermal study of a layer of randomly distributed gold nanoparticles: From nano-localization to macro-scale effects. *J. Phys. D Appl. Phys.* **2017**, *50*, 435302. [CrossRef]
19. Saupe, A. On molecular structure and physical properties of thermotropic liquid crystals. *Mol. Cryst. Liq. Cryst.* **1969**, *7*, 59–74. [CrossRef]
20. Khoo, I.C. *Liquid Crystals*; John Wiley & Sons: Hoboken, NJ, USA, 2007; Volume 64.
21. de Gennes, P.; Prost, J. *The Physics of Liquid Crystals*; Oxford University Press: Oxford, UK, 1993; Volume 83.
22. Khoo, I.C. Nonlinear optics, active plasmonics and metamaterials with liquid crystals. *Prog. Quantum Electron.* **2014**, *38*, 77–117. [CrossRef]
23. Si, G.; Zhao, Y.; Leong, E.S.P.; Liu, Y.J. Liquid-crystal-enabled active plasmonics: A review. *Materials* **2014**, *7*, 1296–1317. [CrossRef] [PubMed]
24. Palermo, G.; Sio, L.D.; Placido, T.; Comparelli, R.; Curri, M.L.; Bartolino, R.; Umeton, C. Plasmonic thermometer based on thermotropic liquid crystals. *Mol. Cryst. Liq. Cryst.* **2015**, *614*, 93–99. [CrossRef]
25. Kimling, J.; Maier, M.; Okenve, B.; Kotaidis, V.; Ballot, H.; Plech, A. Turkevich method for gold nanoparticle synthesis revisited. *J. Phys. Chem. B* **2006**, *110*, 15700–15707. [CrossRef] [PubMed]
26. Perivolari, E.; D'Alessandro, G.; Apostolopoulos, V.; Brouckaert, N; Heiser, T.; Kaczmarek, M. Two-dimensional snapshot measurement of surface variation of anchoring in liquid crystal cells. *Taylor Francis Liq. Cryst.* **2021**, *1*, 1–11.
27. Stöhr, J.; Samant, M.G.; Cossy-Favre, A.; Diaz, J.; Momoi, Y.; Odahara, S.; Nagata, T. Microscopic origin of liquid crystal alignment on rubbed polymer surfaces. *ACS Macromol.* **1998**, *6*, 1942–1946. [CrossRef]
28. Serak, S.V.; Bunning, T.J.; Tabiryan, N.V. Ultrafast photoalignment: Recording a lens in a nanosecond. *Crystals* **2017**, *7*, 338. [CrossRef]
29. Kimball, B.R.; Steeves, D.M.; Hoke, L.; Osgood, R.M.; Carlson, J.; Belton, L.; Tabiryan, N.V.; Rersisyan, S.R.; Serak, S.V.; Hrozhyk, U.A.; et al. *Advances in Anisotropic Materials for Optical Switching*; Technical Report; Massachusetts Inst of Tech Lexington Lincoln Lab: Lexington, MA, USA, 2010.
30. Grillo, R.; Beutel, D.; Cataldi, U.; Rockstuhl, C.; Bürgi, T. Self-Assembled Arrays of Gold Nanorod-Decorated Dielectric Microspheres with a Magnetic Dipole Response in the Visible Range for Perfect Lensing and Cloaking Applications. *ACS Appl. Nano Mater.* **2020**, *3*, 6108–6117. [CrossRef]
31. Fu, Q.; Sun, W. Mie theory for light scattering by a spherical particle in an absorbing medium. *Appl. Opt.* **2001**, *40*, 1354–1361. [CrossRef] [PubMed]
32. Pezzi, L.; De Sio, L.; Veltri, A.; Placido, T.; Palermo, G.; Comparelli, R.; Curri, M.L.; Agostiano, A.; Tabiryan, N.; Umeton, C. Photo-thermal effects in gold nanoparticles dispersed in thermotropic nematic liquid crystals. *Phys. Chem. Chem. Phys.* **2015**, *17*, 20281–20287. [CrossRef] [PubMed]